IEEE Access
Multidisciplinary | Rapid Review | Open Access Journal

Date of publication xxxx 00, 0000, date of current version xxxx 00, 0000.

Digital Object Identifier 10.1109/ACCESS.2022.Doi Number

Mutual Coupling Reduction of a Circularly Polarized MIMO Antenna Using Parasitic Elements and DGS for V2X Communications

MD. ABU SUFIAN[1], NIAMAT HUSSAIN[2], (Member, IEEE), ANEES ABBAS[1], JAEMIN LEE[1], SEONG GYOON PARK[3], AND NAM KIM[1,*]

[1]School of Information and Communication Engineering, Chungbuk National University, Cheongju 28644, South Korea
[2]Department of Smart Device Engineering, Sejong University, Seoul 05006, South Korea
[3]Department of Information and Communication Engineering, Kongju National University, Gongju 314701, South Korea

[*]Corresponding author: Nam Kim (e-mail: namkim@chungbuk.ac.kr).

This work was supported by the Institute for Information and Communications Technology Promotion (IITP), funded by the Korean government (MSIP) (No. 2021-0-00490, Development of precision analysis and imaging technology for biological radio waves).

ABSTRACT In this article, a 4-port circularly polarized (CP) multiple-input multiple-output (MIMO) antenna at 5.9 GHz is presented for the vehicle to everything (V2X) communications. A novel hybrid decoupling structure consisting of circular ring parasites and defected ground structure (DGS) is used to reduce the mutual coupling between the MIMO elements. The circular ring parasites are incorporated between the antennas to reduce the mutual coupling between perpendicular antennas. Whereas, the DGS significantly reduces the mutual coupling between adjacent antennas. These circular ring parasites and DGS affect the electromagnetic field distribution and consequently reduce the mutual coupling. The effectiveness of the decoupling structure is explained through transmission coefficient and surface current distribution. The simulated and measured results show that the proposed MIMO antenna provides overlapping S_{11} (–10 dB) and axial ratio (3-dB) bandwidth of 2.04% (5.82 – 5.94 GHz) with a peak gain of 7.68 dBic. Moreover, the fabricated MIMO antenna offers excellent diversity performance, isolation between antenna elements is very high (>34dB), envelope correlation coefficient (ECC) is lower than 0.001, and diversity gain is 9.99 dB, very close to the ideal value of 10 dB. Furthermore, the link budget for the proposed MIMO system is calculated to check the suitability for V2X communications which shows that the antenna can communicate between them over a distance of 1.5 kilometers with a 21 dBm of transmit power. Owing to these qualities, the proposed MIMO antenna can be an excellent choice for V2X MIMO communications.

INDEX TERMS MIMO antenna, V2X communication, circularly polarized antenna, isolation enhancement, decoupling structure, parasitic element, DGS, link budget.

I. INTRODUCTION

Vehicular communication is gaining popularity in academics and industry for Intelligent Transportation Systems to enhance road safety and traffic efficiency [1]. The vehicle-to-everything (V2X) communication technology system enables vehicles to communicate between vehicles, traffic, and the environment around them using short-range wireless signals [2]. For V2X communication, the Federal Communication Commission (FCC) recommended the 5.9 GHz frequency band [3]. Moreover, the 3rd Generation Partnership Project (3GPP) and 5G Automotive Association (5GAA) both organizations also targeted the 5.9 GHz frequency band for V2X communication [4], [5]. All over the world, the frequency band from 5.850 – 5.925 GHz is mostly used for V2X communication shown in Fig.1 [1], [3]–[6].

The circularly polarized MIMO antennas are considered as a better solution for V2X communication systems. In terms of signal propagation, CP has numerous significant benefits over linear polarization (LP). For example, CP antennas propagate in two orthogonal directions, allowing transmitting and receiving antennas with the same signal power to be oriented freely [7]. Furthermore, CP antennas outperform LP antennas in terms of immunity to multipath distortions, fading, and interferences [8]. These are the reasons the CP is a popular choice for wireless and satellite

Countries	Spectrum (GHz)	Allocated Bandwidth(MHz)
Korea	5.855 – 5.925	70
Japan	0.7555 – 0.7645	9
	5.770 – 5.850	80
China	5.905 – 5.925	20
Singapore	5.875 – 5.925	50
EU	5875 – 5.925	30
USA	5.850 – 5.925	75
Australia	5.855 – 5.925	70

FIGURE 1. Global snapshot of the V2X communication spectrum [3]-[6].

communication, 4G/5G communication, particularly in wireless sensors, randomly oriented RFID tags, and device-to-device communication systems [9]. The CP radiation of the patch antenna could be obtained by optimizing truncated corner square patches [7], perturbation segment to the patch [10,11,12], coupling with unequal orthogonal slot [13] or dual feeding with 90° phased shifts [14].

In recent years, MIMO systems are rapidly adopted in communication technologies. By regulating the signal propagation phase over several antennas, MIMO technology allows operators to electronically control the directivity of an RF signal [15]. Additionally, by spatial multiplexing, MIMO can increase data-carrying capacity without requiring extra bandwidth [16]. Also, the diversity performances can be achieved without multipath distortion by using the MIMO antenna technology [17]. However, the correlation of MIMO antenna elements affects by the mutual coupling between antenna elements, thereby lowering the data rate [18]. Hence, the development of the MIMO antenna with a very low mutual coupling has become a major concern in both academics and industry. Various types of mutual coupling reduction techniques have been reported in the literature [19]–[33]. The generated mutual coupling among MIMO antenna components can be minimized by using different decoupling mechanisms such as meta-material [19], modified array antenna decoupling surface [20], and near-field resonator [21]. However, these structures [19]–[21] mostly increase the antenna profile. In addition, various DGS incorporating slots and stubs along with shorting pins have been utilized to increase MIMO antenna isolation, grounded stubs with DGS [22], slots and matching stubs [23], split ground plane [24], coplanar defected ground plane [25], slots and shorting pins [26]. The presented antennas in [23], [24] occupy a larger substrate size and [25] provide a very low peak gain while antenna [26] provide high isolation and high gain but have disadvantages of the antenna fabrication complexity. The effects of parasitic components on the mutual coupling of MIMO antennas are investigated in [27] by placing several square parasitic elements in the near vicinity to MIMO elements. Another way to reduce mutual coupling is the band-stop filter [28], [29]. In [28], a resonator-based band-stop filter is used as a decoupling network whereas a matrix-based band-stop filter is used to reduce the mutual coupling between antenna elements [29]. While a metamaterial absorber structure is used to achieve high isolation between two patch antennas [30]. However, the techniques reported in [27]–[30] are especially used for linearly polarized antennas and do not consider the situation where the patches are arranged orthogonally to achieve orthogonal polarization.

In this article, we propose a novel hybrid decoupling structure consisting of circular ring parasites and DGS to reduce the mutual coupling of a circularly polarized MIMO antenna. A truncated corner square patch is used to produce the circular polarization which is fed by a quarter-wave matching feedline. All the antenna parameters of the proposed MIMO antenna including the link budget make it promising for the V2X communication system. The main attribute of this work is a very low mutual coupling among the MIMO antenna parts while offering circular polarization and high gain. By creating a well-designed arrangement of the circular ring parasites and DGS, the mutual coupling is reduced significantly. The rest of the paper is organized as follows. Section-II illustrates single element antenna geometrical specifications, design method, CP generation techniques, and results. Also, the design procedure of the proposed MIMO antenna, and the proposed mutual coupling reduction techniques are explained in detail in Section II. While, in Section-III, simulated and measured results, diversity parameters, and link budget of the proposed circularly polarized MIMO antenna is presented along with a performance comparison of the proposed work with previous works. The proposed work is finally concluded in Section IV.

II. ANTENNA CONFIGURATION AND DESIGN PROCESS

A. SINGLE ELEMENT ANTENNA

Fig. 2(a) represents the geometry of the single element antenna. The antenna is made up of a square patch radiator which is connected with a quarter-wave matching feedline followed by a 50-Ω microstrip line, a ground plane, and a Rogers RT5880 substrate ($\varepsilon_r = 2.2$ and $tan\delta = 0.0009$) with the thickness of $h = 1.524$ mm. A 50-Ω coaxial cable is used to feed the microstrip line. The opposite corner of the square patch is truncated to generate circular polarization. The antenna is designed to resonate at the targeted frequency $f_r \approx 5.9$ GHz. The preliminary size of the square patch is predicted as [31]:

$$P = \frac{c}{2f_r}\sqrt{\frac{2}{\varepsilon_r+1}} \quad (1)$$

Here, c denotes the speed of light in empty space and the dielectric constant of the substrate is ε_r. The parameters of the antenna are optimized for the desired performances especially impedance bandwidth, AR bandwidth, radiation efficiency, and gain. The optimal parameters of the single element antenna are as follows: a = 32, b = 52 mm, P = 16.3 mm, w_1 = 4.85 mm, w_2 = 1.51 mm, E = 13.575 mm, l_1 = 17.41 mm, l_2 = 9.85 mm, and c = 3.96 mm. The fabricated prototype of the single element antenna is shown in Fig. 2(b). The measurement instruments and procedure are the same as explained for the proposed MIMO antenna later in Section-IV.

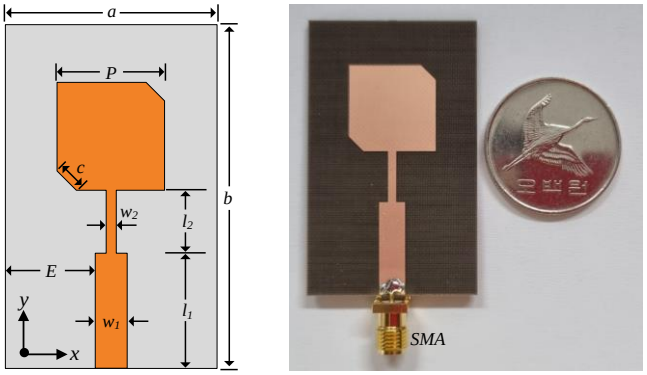

FIGURE 2. **Single element antenna (a) geometry and configuration, and (b) fabricated prototype.**

The simulated and measured results of the single element antenna are shown in Fig. 3. A good agreement is observed between the simulated and measured results. The single element antenna offers – 10 dB impedance bandwidth of 7.74 % (5.59 – 6.04 GHz), and 3-dB axial ratio bandwidth of 120 MHz (5.82 – 5.94 GHz) as seen in Fig. 3(a). The offered bandwidth of the single element antenna covers the whole desired V2X communication spectrum. In Fig. 3(b), the gain and radiation efficiency of the single element is illustrated. The antenna offers a maximum stable gain of 7.68 dBic and radiation efficiency of more than 94% at the entire operating frequency. The measurement value of gain and radiation efficiency is slightly lower than the simulated values due to the measurement equipment losses.

B. PROPOSED MIMO ANTENNA

The geometry and configurations of the proposed 4-port (2×2) MIMO antenna are shown in Fig. 4, which is made up of four single-element antennas that are arranged in an orthogonal pattern on a single substrate. The minimum inter-element spacing between the MIMO antenna elements is E_s = 8.65 mm. The proposed hybrid decoupling structure is the combination of a novel DGS structure in the ground plane and a novel circular ring parasitic structure between the antenna elements. The proposed DGS structure significantly reduces the mutual coupling between adjacent antennas. Whereas the proposed circular ring parasitic structure reduced the mutual coupling between perpendicular antennas. And their combined effect

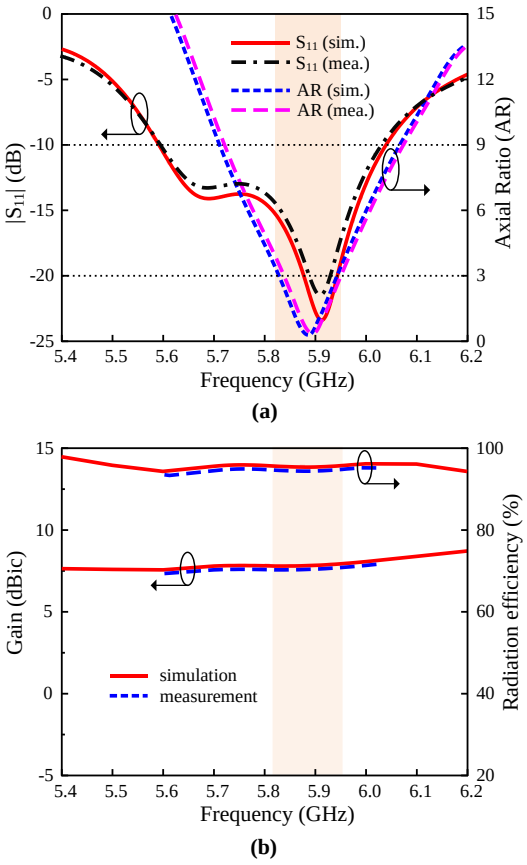

FIGURE 3. **Single element antenna results (a) reflection coefficient, axial ratio (AR), (b) gain, and radiation efficiency.**

offers very high isolation between the MIMO elements. Those results are shown in the later sections and the step-by-step design procedure of the proposed MIMO antenna are explained in the following sub-section. The optimum values for the proposed MIMO antenna parameters are listed in Table 1.

TABLE 1. **Dimensions of the proposed CP-MIMO antenna.**

Parameter	Value (mm)	Parameter	Value (mm)	Parameter	Value (mm)
A	74	j	2.5	r_4	5
P	16.3	k_1	25	r_5	1.5
w_1	4.85	k_2	46.5	r_6	3
w_2	1.51	g_1	0.1	d_1	3
l_1	17.41	g_2	1	d_2	9
l_2	9.85	g_3	1.05	s_1	22
c	3.96	r_1	7	s_2	21.18
h	1.575	r_2	9.5	s_3	9.95
i	2.5	r_3	2.5	s_4	8.95

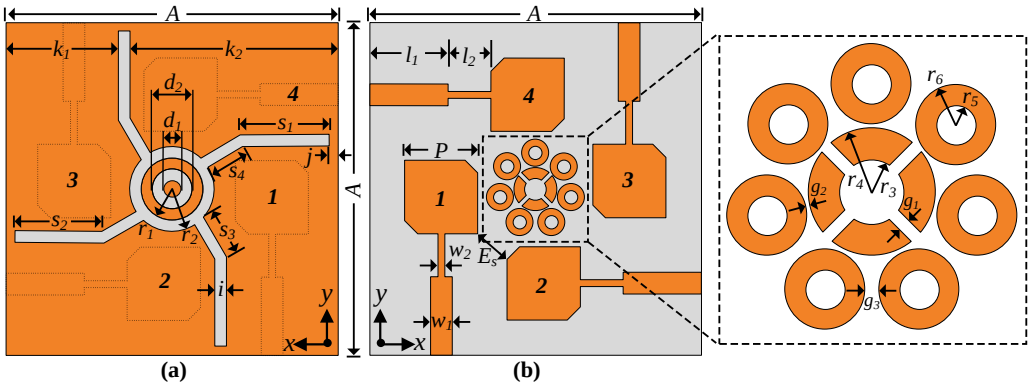

FIGURE 4. Geometry and configuration of the proposed MIMO antenna (a) ground plane, and (b) top view of patch.

C. MIMO ANTENNA DESIGN PROCEDURE

1) MIMO ANTENNA WITHOUT DECOUPLING STRUCTURE

The MIMO antenna consists of four single-element antennas that are arranged orthogonally to one another. The single elements are placed orthogonally to obtain polarization diversity. The MIMO antenna is created by rotating the single-element, *z*-axis 90°, and changing the values of *m* and *m*+10 at the *y*-axis and *x*-axis, respectively, where *m* is the adjustment parameter of the orthogonal placement, with a repetition factor of three. All properties and parameters of the single element antenna are unchanged, only the size of the shared substrate is increased. Without adopted any decoupling structure the optimum parameter values for the MIMO antenna are: A = 74mm, m = 11 mm, P = 16.3 mm, w_1 = 4.85 mm, w_2 = 1.51 mm, l_1 = 17.41 mm, l_2 = 9.85 mm, and c = 3.96 mm.

This antenna offers high mutual coupling between antenna elements, which is expressed by the transmission coefficient, shown in Fig. 5. The transmission coefficient for the adjacent antennas, S_{12}, S_{14}, S_{23}, and S_{34} show identical curves. Similarly, the perpendicularly located antennas, S_{13}, and S_{24} curves are the same. The mutual coupling of the MIMO antenna elements reduces the MIMO performances and lowers the data rate. The isolation level of 20 dB might be enough for general communications. However, seamless connectivity with a high data rate is crucial for V2X communication systems. To ensure high data and uninterrupted communication, modulation transmission requires about an SNR of 30 dB in an additive white Gaussian noise (AWGN) channel and, therefore, the mutual coupling should be below −30 dB in V2X communications [1], [18].

2) MIMO ANTENNA WITH DGS

Defected ground structure (DGS) is a very effective way to reduce mutual coupling between printed MIMO antennas. In literature, various types of DGS are used to establish a high level of coupling separation between the MIMO antenna elements [24]–[26]. In this work, a novel defected ground structure is designed to reduce the mutual coupling. The proposed DGS structure is designed by etching out the copper layer from the ground plane, two circular rings at the center, and four boomerang-shaped stubs connected to the bigger ring.

Using the proposed DGS, the mutual coupling between adjacent antennas (S_{12}, S_{14}, S_{23}, and S_{34}) is reduced significantly at the higher frequency shown in Fig. 5.

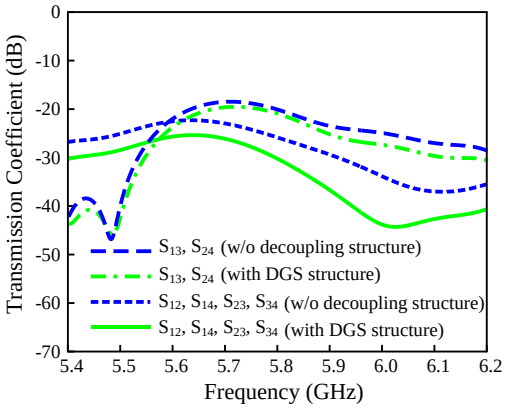

FIGURE 5. The transmission coefficient of the MIMO antenna without decoupling structure and with DGS structure.

However, the mutual coupling between perpendicular antennas (S_{13} and S_{24}) is not improved. Therefore, another method is investigated, which is explained in the later section. The individual effect of circular rings and boomerang-shaped stubs in the ground plane is shown in Fig. 6, only for the adjacent antennas (S_{12}, S_{14}, S_{23}, and S_{34}), as these structures do

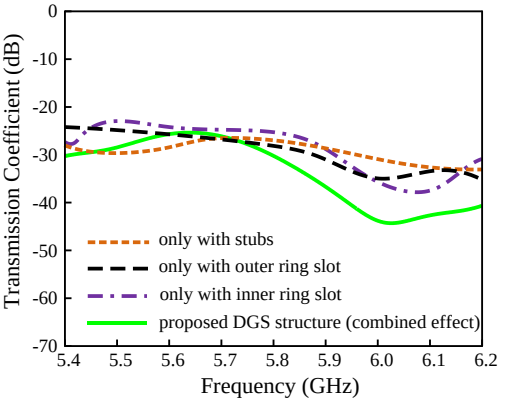

FIGURE 6. The transmission coefficient (S_{12}, S_{14}, S_{23}, and S_{34}) for different DGS structures.

not show any significant effect on perpendicular antennas (S_{13} and S_{24}).

3) MIMO ANTENNA WITH PARASITIC ELEMENTS

In [27], the effects of parasitic elements on the mutual coupling of MIMO antenna are investigated by adding multiple square parasitic elements in close proximity to MIMO elements. In this work, a novel circular ring parasitic structure is proposed. The inner ring is designed by the inner

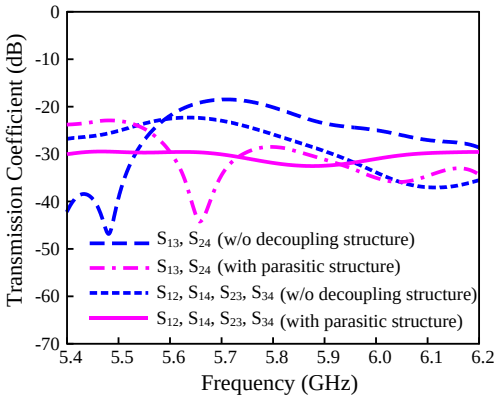

FIGURE 7. The transmission coefficient of the MIMO antenna without decoupling structure and with parasitic structure.

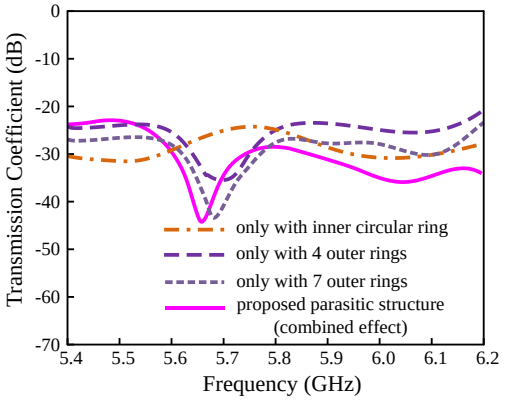

FIGURE 8. The transmission coefficient (S_{13}, and S_{24}) for different parasitic structures.

radius and outer radius of r_3 and r_4, respectively. The inner ring is separated on four places with a distance of g_1. Seven smaller rings are placed in close proximity to the inner ring with the inner radius of r_5, and outer radius of r_6, while they maintain a distance of g_3 between them. In detail dimensions and parameters of the proposed circular ring parasites are presented in Fig. 4 and Table. 1, respectively.

Fig. 7 shows the transmission coefficient of the MIMO antenna with parasitic structure. The proposed circular ring parasitic structure reduces the mutual coupling between the perpendicular antennas (S_{13} and S_{24}). Also offers better performances for the adjacent antennas (S_{12}, S_{14}, S_{23}, and S_{34}), than the MIMO antenna without decoupling structure. The independent effect of different components of the proposed circular ring parasitic structures for perpendicular antennas (S_{13} and S_{24}) is illustrated in Fig. 8.

4) PROPOSED MIMO ANTENNA WITH HYBRID DECOUPLING STRUCTURE

For the designed MIMO antenna, the DGS structure offers better performances for adjacent antennas, whereas the proposed parasitic structure provides better isolation for perpendicularly placed antennas. Hence, both techniques are combined, and a hybrid decoupling mechanism is proposed as illustrated in Fig. 9, to achieve very low mutual coupling between the MIMO elements.

Fig. 10 highlights the mutual coupling reduction by using the proposed hybrid decoupling configuration. It can be seen that, in the operating frequency band, the proposed decoupling structure (DGS and parasitic elements) significantly reduced the coupling effect of the MIMO elements and established high isolation among the adjacent antennas. For the adjacent

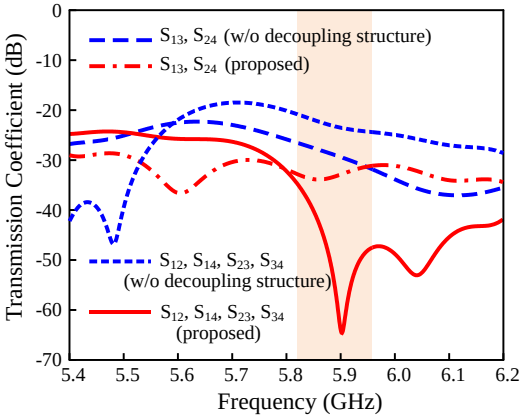

FIGURE 10. Different MIMO configuration's transmission coefficients.

antennas ($|S_{12}|$, $|S_{14}|$, $|S_{23}|$, and $|S_{34}|$) the maximum isolation for MIMO antennas without decoupling configurations is 28 dB, whereas, with the proposed hybrid decoupling configuration for the proposed MIMO system, this level is increased to 65 dB. The best isolation value for perpendicularly situated antenna elements ($|S_{13}$ and $|S_{24}|$) without any decoupling

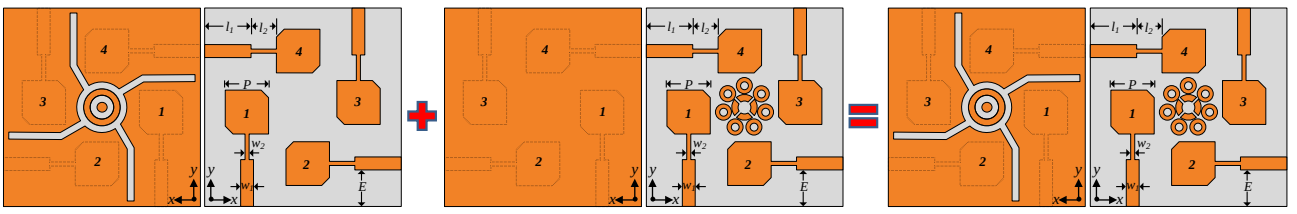

FIGURE 9. Design evolution of the proposed MIMO antenna.

mechanism is 21 dB, however, this value is enhanced to 34 dB after using the hybrid decoupling structure.

The decoupling structure's efficacy can also be determined by observing the surface current distribution [26]. The surface current distribution for the different exciting ports of the proposed MIMO antenna at frequency 5.9 GHz is shown in Fig. 11. While port-1 is activated, as shown in Fig. 11(a), the excited patch induced significant current flow to the nearby elements for the MIMO antenna without a decoupling mechanism, resulting in a very high mutual coupling. On the contrary, the excessive induced current to the surrounding patches is prevented by the proposed decoupling mechanism and reducing mutual coupling among MIMO antenna parts and providing high isolation. Fig. 11(b) shows the surface current distribution for the excited port-3 to confirm that the proposed decoupling structure has the same effect.

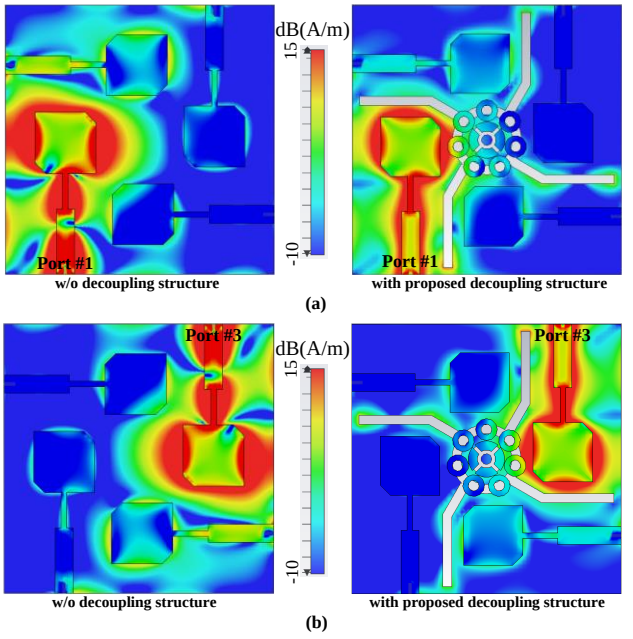

FIGURE 11. Surface current distribution of different port excitation at 5.9 GHz with and without decoupling structure (a) port-1 and (b) port-3.

III. PROPOSED MIMO ANTENNA RESULTS

To evaluate the proposed design, a prototype of the proposed MIMO antenna is manufactured and measured. In Fig. 12, the fabricated antenna photograph and its setup for measurement are shown. All the MIMO antenna elements are connected with a K-connector (50-Ω 2.92mm). A PNA network analyzer(Agilent Technologies E8364B) is used to measure the S-parameters in open-air environments. A commercial institution [33] measures and characterizes the far-field radiation performance of the antenna in an anechoic facility. A well-calibrated regular gain horn antenna is employed as a transmit antenna, while the prototype antenna is used as a receiver. Amplifiers are used to provide constant power reception. During testing, the antenna is rotated to detect the radiation intensity at various angles. The reliability of the proposed MIMO antenna system is determined by examining the diversity performance in the perspective of the transmission coefficient, ECC, diversity gain, mean effective gain (MEG), and channel capacity loss (CCL).

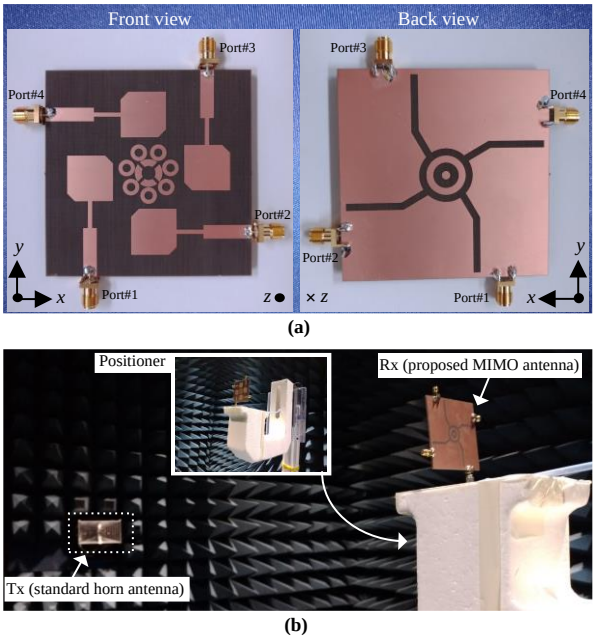

FIGURE 12. Photographs of the (a) fabricated antenna, and (b) far-field measurements setup.

A. REFLECTION COEFFICIENT AND AXIAL RATIO

Reflection coefficient curves of the proposed MIMO antenna, both simulated and measured are shown in Fig. 13. The proposed hybrid structure is included between the MIMO components to reduce mutual coupling, resulting in MIMO antennas with a slightly different S_{11} (–10 dB) bandwidth than single-element antennas. The fabricated prototype offers a –10 dB impedance bandwidth of 7.05% (5.61–6.02 GHz). The simulated and measured findings show a high level of agreement. As shown in Table 2, the antenna offers 3-dB axial ratio bandwidth of 120 MHz (5.82–5.94 GHz). During the measurement of antenna element 1, only port 1 is excited, while the remaining ports are terminated with a 50-Ω load. Similarly, the rest of the antenna elements measurements are made by exciting the corresponding antenna port and connecting the 50- Ω load to other ports.

The offered bandwidth of the proposed MIMO antenna covers the whole desired V2X communication spectrum. The antenna elements show almost similar reflection coefficient and AR bandwidth due to the identical geometry and arrangement of all MIMO antenna elements.

B. TRANSMISSION COEFFICIENT

The mutual correlation between MIMO components is represented by the transmission coefficient. The simulated and measured transmission coefficients of the proposed MIMO antenna are plotted in Fig. 14. The antennas have a very low mutual coupling between the antenna elements when adopting

the proposed hybrid decoupling structure. In the whole operational bandwidth, the antennas have a maximum mutual coupling of 34 dB and a minimum mutual coupling of 65 dB.

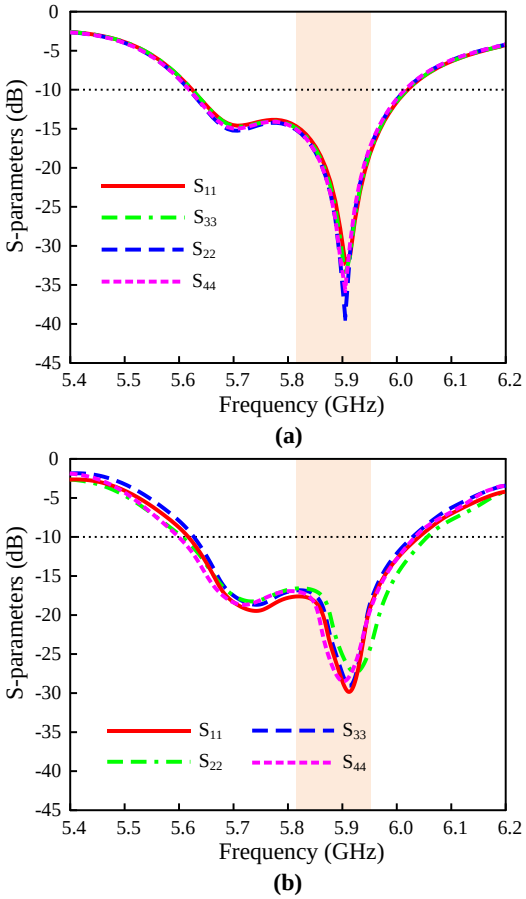

FIGURE 13. **Reflection coefficient of the proposed MIMO antenna (a) simulated and (b) measured.**

C. RADIATION PATTERNS

The simulated and measured radiation patterns of the proposed MIMO antenna at 5.9 GHz in *xoz*-plane and *yoz*-plane for all antenna ports are presented in Fig. 15. For all of the ports tested, the antenna provides steady radiation patterns with low back and side-lobe levels. The antenna offers the RHCP sense of polarization because the LHCP is very negligible as compared to the RHCP showing high polarization isolation. The XPD (cross-polarization discrimination) in CP antennas is the difference between the RHCP and the LHCP levels. The XPD of the proposed CP-MIMO antenna is high (more than 15 dB), as can be seen in the radiation pattern plot in Fig. 15. The antenna port-1 shows a maximum gain of 7.68 dBic with a half-power beamwidth of 91° and 70° at *xoz*-plane and *yoz*-plane, respectively. All the other antenna ports offer the same value of half-power beamwidth, but the planes are different because of the orientation of the elements. As the DGS is very sensitive to the ground plane, the antenna is simulated with a car model to check the antenna performance at practical uses. The antenna is placed 5 mm above the car body. The proposed MIMO antenna shows almost identical performance with the car model. The 3D-radiation pattern of the proposed MIMO antenna with the car model is shown in Fig. 16 while port-1 is excited.

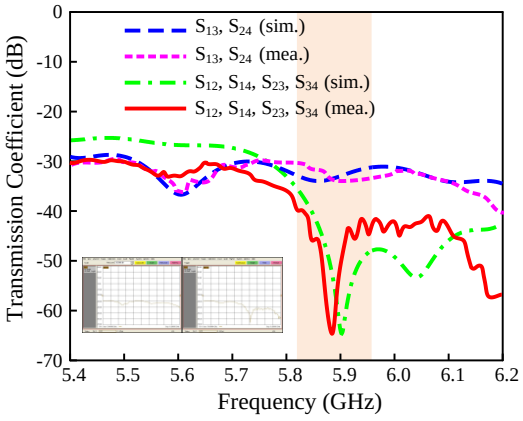

FIGURE 14. **The simulated and measured transmission coefficient of the proposed MIMO antenna.**

D. RADIATION EFFICIENCY AND GAIN

The proposed MIMO antenna elements offer practically identical radiation efficiency and gain to the proposed single element antenna which is explained earlier and shown in Fig. 3(b). The proposed MIMO antenna offers a radiation efficiency of more than 94% at the entire operating frequency. The simulated and measured gains of each antenna element in the proposed CP-MIMO assembly are presented in Table 2. Only port 1 is excited while the remaining ports were terminated with a 50-Ω load, during the measurement of antenna element 1. Similarly, the rest of the antenna elements measurements are made by merely exciting the corresponding antenna port and connecting the 50- Ω load to other ports. The gain values for all antennas are nearly identical, and they are similar to the single element CP-antenna studied in Section II.

TABLE 2. **Axial ratio and gain of the proposed CP-MIMO antenna.**

Port	AR bandwidth (GHz)		Gain at 5.9 GHz (dBic)	
	Simulated	Measured	Simulated	Measured
Port#1	5.82 – 5.94	5.82 – 5.94	7.9	7.68
Port#2	5.82 – 5.94	5.825 – 5.94	7.9	7.67
Port#3	5.82 – 5.94	5.82 – 5.94	7.9	7.70
Port#4	5.82 – 5.94	5.82 – 5.94	7.9	7.66

E. ENVELOPE CORRELATION COEFFICIENT (ECC)

The ECC measures how independent MIMO elements are in terms of performance, such as polarization and radiation patterns [34]. The ECC (ρ_{eij}) of the proposed MIMO antenna system is computed based on S-parameters and far-field radiation by using the equation (2) and (3), respectively [26].

$$\rho_{eij} = \frac{|S_{ii}^{*}S_{ij}+S_{ji}^{*}S_{jj}|^2}{(1-|S_{ii}|^2-S_{ij}^2)(1-|S_{ji}|^2-S_{jj}^2)} \quad (2)$$

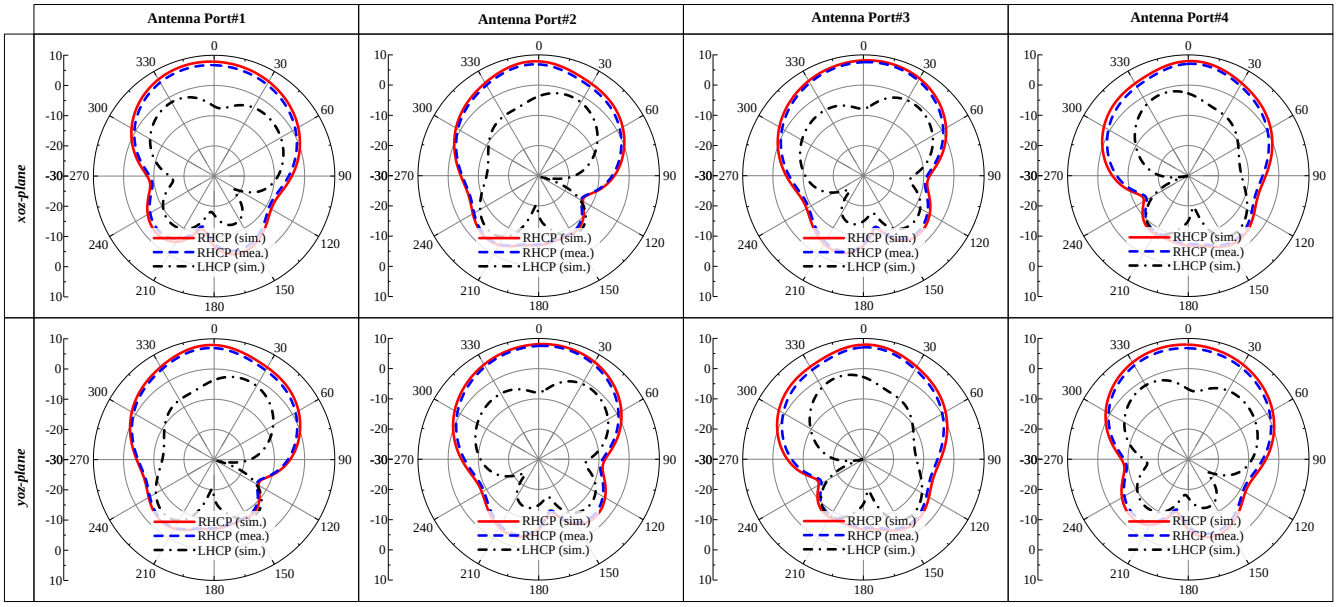

FIGURE 15. Proposed MIMO antenna radiation pattern at 5.9 GHz for all port excitations.

$$\rho_{eij} = \frac{|\iint_0^{4\pi}[\overrightarrow{R_i}(\theta,\varphi)\times\overrightarrow{R_j}(\theta,\varphi)]d\Omega|^2}{\iint_0^{4\pi}|\overrightarrow{R_i}(\theta,\varphi)|^2 d\Omega \iint_0^{4\pi}|\overrightarrow{R_j}(\theta,\varphi)|^2 d\Omega} \quad (3)$$

Where, the reflection coefficient is S_{ii}, while the transmission coefficient is S_{ij}. The 3D radiation values of i^{th} and j^{th} antennas are $\overrightarrow{R_i}(\theta,\varphi)$ and $\overrightarrow{R_j}(\theta,\varphi)$, respectively, and the solid angle is expressed by Ω. The ECC values obtained for the proposed MIMO antenna from (2) and (3) are less than 0.001 within the operating frequency. Fig. 17(a) shows this outstanding diversity performance of the proposed MIMO antenna.

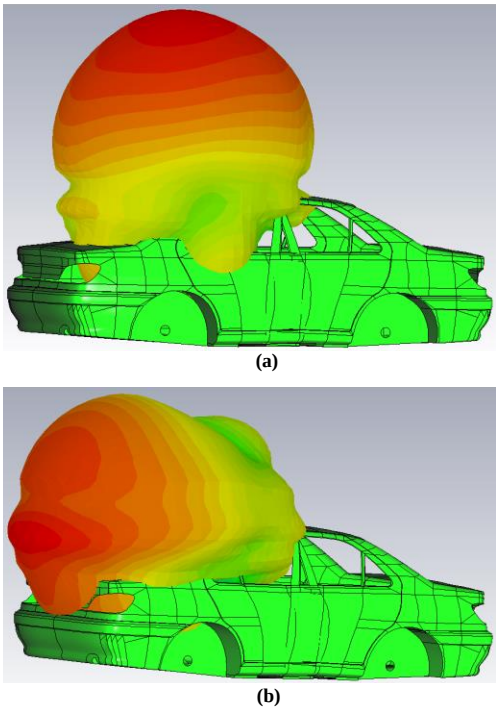

(a)

(b)

FIGURE 16. The 3D-Radiation pattern of the proposed MIMO antenna with the car model at 5.9 GHz while port-1 is excited (a) horizontal arrangement and (b) vertical arrangement.

F. DIVERSITY GAIN (DG)

Another important parameter is the DG, which indicates how the diversity scheme of MIMO antennas affects the radiated power. For the proposed MIMO antenna the DG is calculated from the value of S-parameters using equation 4 [26] and shown in Fig. 17(b).

$$Diversity\ Gain = 10\sqrt{1-|\rho_{eij}|^2} \quad (4)$$

The proposed MIMO antenna offers a diversity gain of more than 9.99 dB for all the antenna elements, which value is almost similar to the ideal value.

G. MEAN EFFECTIVE GAIN (MEG)

The MEG, which is a ratio of the mean received power to the mean incident power of the antenna, is another significant statistic to quantify diversity performance in MIMO systems [36]. The acceptable practical value of MEG should be within –3 dB to –12 dB range [37]. For our proposed MIMO system, the MEG value is calculated by using the equation 5 [36], [37]:

$$MEG_i = 0.5\left(1-\sum_{i=1}^{N}|S_{ij}|\right) \quad (5)$$

In this equation, i stand for the observation port, and the antennas number in the MIMO system is represented by N. Fig. 18 explores the MEG for all the ports of the proposed

This article has been accepted for publication in a future issue of this journal, but has not been fully edited. Content may change prior to final publication. Citation information: DOI 10.1109/ACCESS.2022.3177886, IEEE Access

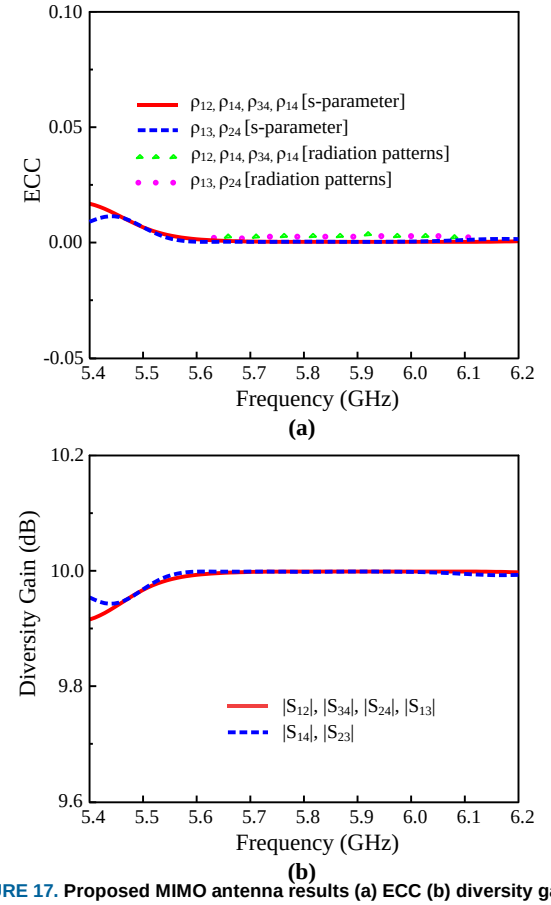

FIGURE 17. **Proposed MIMO antenna results (a) ECC (b) diversity gain.**

MIMO system. The MEG values are less than -7 dB within the operating frequency band.

H. CHANNEL CAPACITY LOSS (CCL)

The CCL is a metric that estimates the maximum amount of channel loss that allows a message to be successfully transmitted over a communication channel. For reliable communication, the CCL should not exceed 0.4 bits/s/Hz. Equations (6) and (7) provide the formulas for calculating the CCL [7], [36]. Where, correlation matrix of the MIMO antenna elements is M_{ANT}, and $\rho_{ii} = 1 - (|S_{ii}|^2 - |S_{ij}|^2)$ and $\rho_{ij} = -(S_{ii}^* S_{ij} + S_{ji}^* S_{ij})$ for $i, j = 1, 2, 3$ or 4. Fig. 19 shows the CCL value at the intended transmission frequency was significantly less than 0.15 bits/s/Hz.

$$CCL = -log_2 \det|M_{ANT}| \tag{6}$$

$$M_{ANT} = \begin{bmatrix} \rho_{11} & \rho_{12} & \rho_{13} & \rho_{14} \\ \rho_{21} & \rho_{22} & \rho_{23} & \rho_{24} \\ \rho_{31} & \rho_{32} & \rho_{33} & \rho_{34} \\ \rho_{41} & \rho_{42} & \rho_{43} & \rho_{44} \end{bmatrix} \tag{7}$$

I. LINK BUDGET

A link budget is a method of quantifying the performance of a communication link while accounting for all the power, gains, and losses that a communication signal experiences in a telecommunication system, from the transmitter to the receiver, via a communication medium such as a waveguide, radio waves, optical fiber, or cable. The proposed MIMO antenna's link budget is calculated to determine its suitability for V2X communication by using the following equation [37]:

$$P_{RX} = P_{TX} + G_{TX} - L_{TX} - L_{FSP} + L_M + G_{RX} - L_{RX} \tag{8}$$

Where, P_{RX} and P_{TX} are the received and transmit power in dBm, respectively, G_{TX} is the transmitter antenna gain in dBic, L_{TX} is the entire system degradation in decibels (dB) at the transmitter, L_{FSP} is the total propagation losses in dB between the transmit and receive antennas, L_M is miscellaneous losses (fade margin, polarization misalignment, etc.) in dB, G_{RX} is the receiver antenna gain in dBic, and, L_{RX} is the overall system loss at the receiver side in dB.

Here, only free space path loss (L_{FSP}) varies with distance (d) and frequency (f), and all other parameters are constant for a specifically designed system. The free space path loss (L_{FSP}) can be calculated as [38]:

$$L_{FSP(dB/km)} = 32.4 + 20log_{10}(d_{km}) + 20Log_{10}(f_{MHz}) \tag{9}$$

MATLAB is used as a tool to calculate the link budget of the proposed MIMO antenna by using the equation (8) and (9)

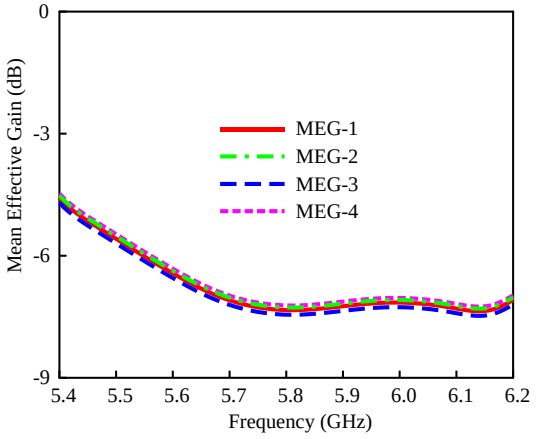

FIGURE 18. **MEG of the proposed MIMO system.**

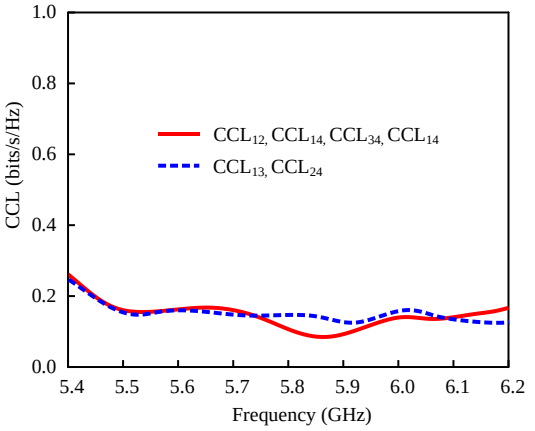

FIGURE 19. **CCL characteristics of the proposed MIMO system.**

TABLE 3. Performance comparison of the proposed CP-MIMO antenna with previous works.

Ref.	No of Ports	Overall Antenna Volume (λ^3)	Center Freq. (GHz)	LP / CP	Mutual Coupling Reduction Techniques	Min. Inter-element Spacing	Max. Gain (dBi)	Radiation Efficiency	Isolation (dB)		ECC
									Min.	Max.	
[20]	2	0.83 × 0.66 × 0.014	4.1	LP	Modified array antenna decoupling surface	0.034λ	7.9	Not given	≥ 25	45	<0.01
[21]	2	1.05 × 0.68 × 0.006	2.25	LP	Near-field resonators	0.016λ	5.11	80%	≥ 20	25	Not given
[22]	2	1.25 × 0.83 × 0.007	2.5	CP	Grounded stubs and DGS	0.064λ	6.1	91.6%	≥ 20	46	<0.003
[23]	4	1.98 × 1.93 × 0.045	8.5	CP	Slots and matching stubs	0.623λ	6.4	Not given	≥ 18	45	<0.25
[24]	4	2.94 × 2.94 × 0.059	11	LP	Split ground plane	0.459λ	5.8	80%	≥ 25	50	<0.02
[25]	4	1.46 × 1.46 × 0.061	11.5	LP	Defected ground structure	0.723λ	6.2	75%	≥ 17	61	<0.08
[26]	4	1.75 × 1.75 × 0.038	3.59	LP	Slots and shorting pins	0.692λ	8.72	92%	≥ 32	72	<0.001
[27]	2	1.44 × 0.90 × 0.028	5.4	LP	Parasitic elements	0.09λ	6.8	95%	≥ 20	40	<0.02
[28]	2	0.38 × 0.19 × 0.014	2.61	LP	SRR-based band stop filter	0.052λ	3.8	84%	≥ 15	38	<0.121
[30]	2	Not Specified	5.5	LP	Metamaterial absorber	0.202λ	7.74	68.03 %	≥ 23	44	< 0.05
[32]	4	1.38 × 1.38 × 0.14	4.15	LP	Metal walls	0.301λ	7.5	>80%	≥ 15	26	< 0.03
[33]	4	2.08 × 2.08 × 0.14	4.15	LP	Shorting Strips	0.554λ	6.8	>84%	≥ 13	25	< 0.05
[35]	4	1.58 × 1.58 × 0.04	7.9	LP	Parasitic decoupler	0.501λ	6.94	Not given	≥ 21	48	>0.001
Prop.	**4**	**1.46 × 1.46 × 0.029**	**5.9**	**CP**	**Parasitic elements & DGS**	**0.170λ**	**7.68**	**94%**	**≥ 34**	**65**	**<0.001**

Here, λ is the wavelength in free space at the center working frequency of that individual reference

while $G_{RX} = G_{TX} = 7.6$ dBic, $L_{TX} \approx 3.2$ dB (combined losses of connectors (0.5), cable (1.7), surge kit (0.5), and mismatch (0.511)), $L_M = 0.5$ dBm, $L_{RX} \approx 2.35$ dB (combined losses of surge kit (0.5), cable (0.85), connectors (0.5), and mismatch (0.511)), and the link budget result is shown in Fig. 20.

The antenna sensitivity or the minimum detectable signal of the antenna is calculated using the equation (10) [39]:

$$MDS = 10Log_{10}\left(\frac{kT}{1mW}\right) + Noise\ Figure + 10Log_{10}(Bandwidth) \quad (10)$$

Where, MDS stands for minimum detectable signal, T is the temperature (290) in Kelvin and, k is Boltzmann's constant (−228 dBW/(kHz)). If we use a 70 MHz channel bandwidth with a 13.8 dB noise figure, then the proposed antenna will offer a minimum of -81.8 dBm of sensitivity.

Since the FCC and WHO (World Health Organization) suggests antenna power up to 1 W in urban areas. Moreover, 5GAA suggests 21 dBm transmit power at the time of antenna testing for the V2X communication system [40], to ensure the antenna's effectiveness in actual usage. The link budget of the proposed MIMO antenna is calculated for different transmit power from 126 mW to 1W shown in Fig. 16. From the link budget graph, it can be seen that the antenna can communicate between them over the distance of 1.5 kilometers with the

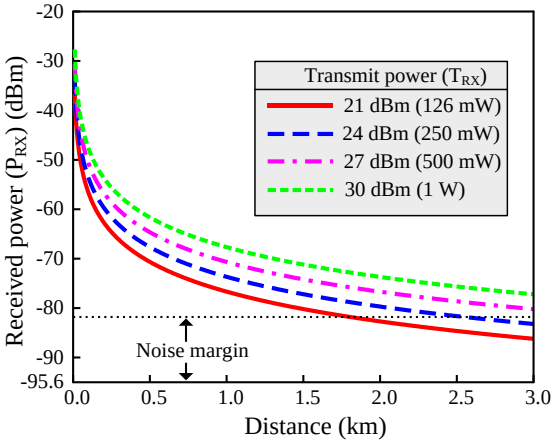

FIGURE 20. Link budget of the proposed MIMO antenna at different transmit power.

minimum Tx power of 21 dBm, whereas the 5GAA asks for a minimum communication distance of 300 meters between the antennas [40].

H. COMPARISON WITH PREVIOUS WORKS

Table 3 compares the proposed CP-MIMO antenna to other similar MIMO microstrip patch designs with significant isolation that have recently been published in the literature. In terms of several performance metrics, the comparison is made including antenna ports, overall antenna volume, center frequency, antenna polarization, mutual coupling reduction techniques, minimum inter-element spacing, maximum gain, radiation efficiency, minimum and maximum isolation, and envelope correlation coefficient (ECC).

It can be seen that a better maximum value of isolation can be achieved by using a decoupling structure, particularly [20], [21], [22], [26], [30]. However, these designs suffer from either low gain and lower number of ports, or cannot offer circular polarization. Our proposed design is superior in terms of ports, radiation efficiency, and the value of ECC with a strong isolation capability. The proposed design is superior in terms of the number of ports, radiation efficiency, and the value of ECC with a strong isolation capability. Also, this antenna offers the lowest inter-element spacing and occupies the lowest overall space among the 4-port MIMO antennas. Furthermore, the proposed MIMO antenna provides high gain and circular polarization while preserving good isolation among the MIMO antenna radiators.

IV. CONCLUSION

A high gain circularly polarized MIMO antenna is presented for V2X communications. A truncated corner square patch is used to produce the circular polarization which is fed by a quarter-wave matching feedline. The low mutual coupling between MIMO antenna elements is the key differentiating characteristic of the proposed design. The overall compact size of the proposed circularly polarized single element antenna design is $0.62\lambda_0 \times 1.0\lambda_0 \times 0.03\lambda_0$. S_{11} (–10 dB) bandwidth of the single antenna element is 7.74% (5.59 – 6.04 GHz), according to simulations and measurements. The antenna also offers a peak gain of 7.68 dBic with a stable and symmetrical radiation pattern and high radiation efficiency (>94%). Using the proposed single element, the MIMO antenna is created by positioning all single elements orthogonally. A novel hybrid decoupling structure consisting of circular ring parasites and defected ground structure is proposed to reduce the mutual coupling between the circularly polarized MIMO elements. The electromagnetic field dispersion is affected by the proposed hybrid decoupling structure, resulting in the high dispersion of induced current to surrounding patches being stopped and good isolation between MIMO antenna elements is accomplished. A prototype of the proposed 2×2 (4-port) MIMO antenna is fabricated and measured to validate the design concept. The overall compact size of the proposed MIMO antenna is $1.4\lambda_0 \times 1.4\lambda_0 \times 0.03\lambda_0$. The simulation and measurement result shows a good agreement. The proposed CP-MIMO antenna has a wide –10 dB impedance bandwidth of 7.05% (5.61 – 6.01 GHz) and a 3-dB axial ratio bandwidth of 2.04% (5.82 – 5.94 GHz) with a stable peak gain of 7.68 dBic. All the diversity performances of the proposed CP-MIMO antenna are excellent, between all the MIMO antenna elements high isolation is achieved (>33 dB), ECC is less than 0.001, diversity gain is almost similar to the ideal value (9.99 dB), and acceptable channel capacity loss (0.15 bits/s/Hz) and mean effective gain (–7 dB). The link budget of the proposed MIMO antenna is also calculated based on the measured results to check its suitability for V2X communication which shows that the antenna can communicate between them over the distance of 1.5 kilometers with 21 dBm of Tx power. All these features of the proposed antenna system make it a suitable candidate for V2X MIMO communications.

REFERENCES

[1] S. Gyawali, S. Xu, Y. Qian, and R. Q. Hu, "Challenges and solutions for cellular based V2X communications," *IEEE Commun. Surveys Tutorials*, vol. 23, no. 1, pp. 222-255, Firstquarter 2021.

[2] G. Naik, B. Choudhury, and J. Park, "IEEE 802.11bd & 5G NR V2X: evolution of radio access technologies for V2X communications," *IEEE Access*, vol. 7, pp. 70169-70184, Jun. 2019.

[3] Federal Communications Commission.(Jun. 2020). *Use of the 5.850-5.925 GHz band*. Accessed: Dec. 10, 2021. [Online]. Available:https://www.federalregister.gov/documents/2020/02/06/2020-02086/use-of-the-5850-5925-ghz-band

[4] 3rd Generation Partnership Project. (Apr. 2021). *5GAA study of spectrum needs for safety related ITS*. Accessed: Dec. 10, 2021. [Online]. Available: https://www.3gpp.org/news-events/partners-news/2188-5gaa-study

[5] 5G Automotive Association.(Oct. 2021). *Updated study of spectrum needs for safety related intelligent transportation systems – day 1 and advanced use* cases. Accessed: Dec. 10, 2021. [Online]. Available: https://5gaa.org/news/study-of-spectrum-needs-for-safety-related-intelligent-transportation-systems-day-1-and-advanced-use-cases/

[6] Qualcomm Technologies Inc. *Improved V2X capabilities for safety and autonomous driving*. Accessed: Dec. 10, 2021. [Online]. Available: https://www.qualcomm.com/products/automotive/c-v2x

[7] N. Hussain, M. Jeong, A. Abbas, and N. Kim, "Metasurface-based single-layer wideband circularly polarized MIMO antenna for 5G millimeter-wave systems," *IEEE Access*, vol. 8, pp. 130293-130304, Jul. 2020.

[8] N. Hussain, M. Jeong, A. Abbas, T. Kim, and N. Kim, "A metasurface-based low-profile wideband circularly polarized patch antenna for 5G millimeter-wave systems," *IEEE Access*, vol. 8, pp. 22127-22135, Feb. 2020.

[9] H. Askari, N. Hussain, D. Choi, M. A. Sufian, A. Abbas, and N. Kim, "An AMC-based circularly polarized antenna for 5G sub-6 GHz communications," *CMC-Computers, Materials Continua*, vol. 69, no. 3, pp. 2997-3013, Apr. 2021.

[10] F. A. Dicandia, S. Genovesi, and A. Monorchio, "Analysis of the performance enhancement of MIMO systems employing circular polarization," *EEE Trans. Antennas Propag.*, vol. 65, no. 9, pp. 4824-4835, Sep. 2017.

[11] N. Hussain, M. J. Jeong, J. Park, and N. Kim, "A broadband circularly polarized fabry-perot resonant antenna using a single-layered PRS for 5G MIMO applications," *IEEE Access*, vol. 7, pp. 42897-42907, Apr. 2019.

[12] L. Malviya, R. K. Panigrahi, and M. Kartikeyan, "Circularly polarized 2× 2 MIMO antenna for WLAN applications," *Progress Electromagn. Research*, vol 66, pp. 97–107, 2016.

[13] M. Akbari, M. M. Ali, M. Farahani, A. R. Sebak, and T. Denidni, "Spatially mutual coupling reduction between CP-MIMO antennas

using FSS superstrate," *Electronics Lett.*, vol. 53, no. 8, pp. 516-518, Apr. 2017.

[14]M. K. Nayan, M. F. Jamlos, and M. A. Jamlos, "MIMO circular polarization array antenna with dual coupled 90° phased shift for point-to-point application," *Microwave Optical Tech. Lett.*, vol. 57, no. 4, pp. 809-814, Apr. 2015.

[15]N. O. Parchin, H. J. Basherlou, Y. I. A. Al-Yasir, A. Ullah, R. A. Abd-Alhameed, and J. M. Noras, "Multi-band MIMO antenna design with user-impact investigation for 4G and 5G mobile terminals," *Sensors*, vol. 19, no. 3, p. 456, Jan. 2019.

[16]Y. Zhang, J.-Y. Deng, M.-J. Li, D. Sun, and L.-X. Guo, "A MIMO dielectric resonator antenna with improved isolation for 5G mm-wave applications," *IEEE Antennas Wireless Propag. Lett.*, vol. 18, no. 4, pp. 747–751, Apr. 2019

[17]M. I. Khan, M. I. Khattak, and M. Al-Hasan, "Miniaturized MIMO antenna with low inter-radiator transmittance and band rejection features," *J. Electromagn. Eng. Sci.*, vol. 21, no. 4, pp. 307-315, Sep. 2021.

[18]X. Chen, S. Zhang, and Q. Li, "A review of mutual coupling in MIMO systems," *IEEE Access*, vol. 6, pp. 24706-24719, May 2018.

[19]K. Yu, Y. Li, and X. Liu, "Mutual coupling reduction of a MIMO antenna array using 3-D novel meta-material structures," *Appl. Comput. Electromagn. J.*, vol. 33, no. 7, pp. 758–763, Jul. 2018.

[20]Z. Niu, H. Zhang, Q. Chen and T. Zhong, "Isolation enhancement in closely coupled dual-band MIMO patch antennas," *IEEE Antennas Wireless Propag. Lett.*, vol. 18, no. 8, pp. 1686-1690, Aug. 2019.

[21]M. Li, B. G. Zhong, and S. W. Cheung, "Isolation enhancement for MIMO patch antennas using near-field resonators as coupling-mode transducers," *IEEE Trans. Antennas Propag.*, vol. 67, no. 2, pp. 755–764, Feb. 2019.

[22]M. Y. Jamal, M. Li, and K. L. Yeung, "Isolation enhancement of closely packed dual circularly polarized MIMO antenna using hybrid technique," *IEEE Access*, vol. 8, pp. 11241-11247, Jan. 2020.

[23]S. Kumar, G. H. Lee, D. H. Kim, H. C. Choi, and K. W. Kim, "Dual circularly polarized planar four-port MIMO antenna with wide axial-ratio bandwidth," *Sensors*, vol. 20, no. 19, pp. 5610, Jan. 2020.

[24]V. S. D. Rekha, P. Pardhasaradhi, B. T. P. Madhav and Y. U. Devi, "Dual band notched orthogonal 4-element MIMO antenna with isolation for UWB applications," *IEEE Access*, vol. 8, pp. 145871-145880, Aug. 2020.

[25]W. Yin, S. Chen, J. Chang, C. Li, and S. K. Khamas, "CPW fed compact UWB 4-element MIMO antenna with high isolation," *Sensors*, vol. 21, no. 8, pp. 2688, Jan. 2021.

[26]M. A. Sufian, N. Hussain, H. Askari, S. G. Park, K. S. Shin, and N. Kim, "Isolation enhancement of a metasurface-based MIMO antenna using slots and shorting pins," *IEEE Access*, vol. 9, pp. 73533-73543, May 2021.

[27]H. H. Tran, and N. Nguyen-Trong, "Performance enhancement of MIMO patch antenna using parasitic elements," *IEEE Access*, vol. 9, pp. 30011-30016, Feb. 2021.

[28]H. Islam, S. Das, T. Ali, P. Kumar, S. Dhar, and T. Bose, "Split ring resonator-based bandstop filter for improving isolation in compact MIMO antenna," *Sensors*, vol. 21, no. 7, pp. 2256, Jan. 2021.

[29]B. Tütüncü, "Mutual coupling reduction using coupling matrix based band stop filter," *AEU-Int. J. Electron. Commun.*, vol. 124, pp. 153342, Sep. 2020.

[30]P. Garg, and P. Jain, "Isolation improvement of MIMO antenna using a novel flower shaped metamaterial absorber at 5.5 GHz WiMAX band," *IEEE Trans. Circuits Systems*, vol. 67, no. 4, pp. 675-679, Apr. 2020.

[31]*Antenna Theory: Analysis and Design*, 3rd ed. Hoboken, NJ, USA: Wiley, 2005, pp. 811–820.

[32]K. -L. Wong, X. -Q. Ye, and W. -Y. Li, "Wideband four-port single-patch antenna based on the quasi-$TM_{1/2,1/2}$ mode for 5G MIMO access-point application," *IEEE Access*, vol. 10, pp. 9232-9240, Jan. 2022.

[33]K. -L. Wong, J. -Z. Chen, and W. -Y. Li, "Four-port wideband annular-ring patch antenna generating four decoupled waves for 5G multi-input-multi-output access points," *IEEE Trans. Antennas Propag.*, vol. 69, no. 5, pp. 2946-2951, May 2021.

[34]*EMTI Homepage*. Accessed: Dec. 12, 2021. [Online]. Available: http://emti.or.kr/

[35]S.-H. Kim and J.-Y. Chung, "Analysis of the envelope correlation coefficient of MIMO antennas connected with suspended lines," *J. Electromagn. Eng. Sci.*, vol. 20, no. 2, pp. 83–90, Apr. 2020.

[36]A. Abbas, N. Hussain, M.A. Sufian, J. Jung, S.M. Park, and N. Kim, "Isolation and gain improvement of a rectangular notch UWB-MIMO antenna," *Sensors*, vol. 22, no. 4, pp. 1460, Feb. 2022.

[37]S. Tariq, S. I. Naqvi, N. Hussain, and Y. Amin, "A metasurface-based MIMO antenna for 5G millimeter-wave applications," *IEEE Access*, vol. 9, pp. 51805-51817, Apr. 2021.

[38]A. Kiourti and K. S. Nikita, "Miniature scalp-implantable antennas for telemetry in the MICS and ISM bands: design, safety considerations and link budget analysis," *IEEE Trans. Antennas Propag.*, vol. 60, no. 8, pp. 3568-3575, Aug. 2012.

[39]J. Walfisch and H. L. Bertoni, "A theoretical model of UHF propagation in urban environments," *IEEE Trans. Antennas Propag.*, vol. 36, no. 12, pp. 1788-1796, Dec. 1988.

[40]EverythingRF. *Minimum Detectable Signal Calculator*. Accessed: Dec. 16, 2021. [Online]. Available: https://www.everythingrf.com/rf-calculators/minimum-detectable-signal-calculator

[41]5G Automotive Association (5GAA). *V2X Functional and Performance Test Procedures – Selected Assessment of Device to Device Communication Aspects*. Accessed: Dec. 16, 2021. [Online]. Available: https://5gaa.org/wp-content/uploads/2018/10/5GAA_P-180092_TR_V2X_FP_Test_Procedures_v1.1.pdf